Chapter 2
Measurement and Simulation of Combustion Noise emitted from Swirl Burners

C. Bender, F. Zhang, P. Habisreuther, H. Büchner and H. Bockhorn

Abstract A major uncertaincy, when designing combustors is the influence of geometrical patterns of the design on the combustion noise generated. In order to determine the mechanisms and processes that influence the noise generation of flames with underlying swirling flows, a new burner has been designed, that offers the possibility to vary geometrical parameters. Experimental data (flow field, noise emission) have been determined for this burner. In addition, Large Eddy Simulations (LES) have been performed to study the isothermal and reacting flow of the burner. The results of the measurements show a distinct rise of the sound pressure level, obtained by changing the test setup from the isothermal to the flame configuration as well as by varying geometrical parameters, which is also resembled by the LES simulation results. A physical model has been developed from experiments and verified by the LES simulation, that explains the formation of coherent flow structures and allows to separate their contribution to the overall noise emission from ordinary turbulent noise sources. The computed isothermal and reacting flow fields have been discussed through flow visualization; the computed acoustic pressure has been compared with the experiment and it showed good agreement.

2.1 Introduction

The development of modern gas turbines and jet engines is focused on the reduction of pollutant emissions and, increasingly, on the reduction of overall noise emission, including combustion noise. This requires the minimization of the noise sources, namely noise from the turbulent flow, combustion noise and noise caused by periodic instabilities and fluctuations of the ignition zone. This has to be achieved under

C. Bender, F. Zhang, P. Habisreuther, H. Büchner, H. Bockhorn
University of Karlsruhe, Division of Combustion Technology
Engler-Bunte-Ring 1, 76131, Karlsruhe, Germany
e-mail: feichi.zhang@vbt.uni-karlsruhe.de, christian.bender@vbt.uni-karlsruhe.de

A. Schwarz, J. Janicka (eds.), *Combustion Noise*, DOI 10.1007/978-3-642-02038-4_2,

conservation of the benefits of swirl flames, e.g. high ignition stability and broad operation ranges. Subproject 2 ”Measurement and Simulation of Combustion Noise emitted from Swirl Burners with different Burner Exit Geometries” is focused on the description and characterization of fluctuations of the ignition zone due to different mixing and stabilization characteristics of swirl flames, the influence of the enclosure of the flames in combustion chambers and the description of flame noise caused by the formation and burning of coherent, periodic flow structures, often detected in swirl flows and flames [3, 4, 18, 25].

Most technical combustion systems use turbulent premixed or non-premixed swirl flames with high volumetric reaction densities. To realize good ignition stability, especially, when using high air equivalence ratio to prevent thermal NOx-emissions, the flow field is swirl stabilized. The swirl flow forms - when a critical value of the swirl number is exceeded - a central inner recirculation zone and causes a longer residence time of reactive species and enables the formation of short flames of high reaction densities with the benefits of high ignition stability due to the recirculation of hot gases [5, 23] and the achievable low-pollution combustion. Another advantage of premixed swirl-stabilized flames is the option to reduce pollutant emissions of modern combustion systems materialized in industrial, traffic, power plant and aircraft applications compared to diffusive flames by cost-efficient design solutions. Basic research investigation of swirl flames is given by [16, 21].

Besides the named properties of swirl flames, also some issues arise putting this type of burner into action. Swirl flows and flames tend to generate periodic flow instabilities, which lead to an increasing noise emission and problem of flame stability. Combustion instabilities have been investigated intensively in the recent years using pulsated inflows [1, 9]. Instabilities in swirl flames have been investigated by [10, 22, 28] and reveal the importance of coherent structures in the forward flow surrounding the inner recirculation zone. The existence and the influence of coherent structures on the noise emission of the flame and thus of the combustion system requires more physical knowledge to minimize combustion noise in modern industrial and aircraft applications already during the design process. Another disadvantage of swirl flames are their high noise levels caused by high reaction densities and amplified by the use of premixed flames in industrial furnaces.

Numerical methods using high resolution techniques for the description of turbulent flows, like large eddy simulation (LES) offer the possibility to resolve the unsteady flow structure with high accuracy. The present work uses the LES to adress the mechanisms of the reacting flow field. In this approach, the filtered unsteady Navier-Stokes equations are taken into account and only large scale turbulences are resolved dependent on the cut-off level, the unresolved small ones are modelled via a so-called sgs (subgrid scale)-model. Since the large turbulent motions carry the most energy of the flow and generally show a non-isotropic behaviour, it is adequate to model the small eddies, whereas these exhibit more universal features. Thus, the LES technique is well suited for studying instabilities in the combustor devices, since the flow field of concern is highly unsteady and dominated by turbulence motions that can be adequately resolved computationally [27].

2.2 Theoretical Background

2.2.1 Experimental Setup

The investigations were carried out using a modular double-concentric swirl-burner for premixed and non-premixed combustion of gaseous fuels, offering the options to vary independently geometric parameters (especially the angle of the burning gas injection and the burner exit geometry with a recessed pilot often used in industrial applications [12, 20]) as well as technically relevant operation parameters like thermal load $\dot{Q}_{th}$ and air equivalence ratio $\lambda = \dot{V}_{air}/(\dot{V}_{fuel} \times l_{min})$ with l_{min} as minimal, stoichiometric required air rate. Another advantage of the burner design is the possibility to generate periodic flow instabilities by variation of the burner exit geometry and definite conservation of the mean turbulent flow field [18]. Identical frequencies have been determined in the spectral distributions of the noise far sound field measured by a microphone probe and in the fully turbulent flow field detected via laser diagnostics (Laser Doppler Velocimetry). The part of noise caused by the underlying physical mechanism [25] can be quantified and avoided by proper design of the burner outlet geometry.
The influence of the gas injection angle in the case of non-premixed flames was investigated with variation of gas injection angles between 0^o and 90^o referring to the burner's axis (resulting in type-I and type-II-diffusion flames, see figure 2.13). The operating parameters' range of the pilot burner varied between premixed conditions - leading to sufficient main flame stabilization at the pilot burners exit - and the main flame without pilot flame, causing a fluctuation of the ignition zone in dependence of the gas injection angle of the main gas supply and a strong corresponding increase of the flame noise.
Figure 2.1 shows a sketch of the double-concentric burner, which produces two concentric swirl-flows: A central pilot burner flow and an outer main burner flow.

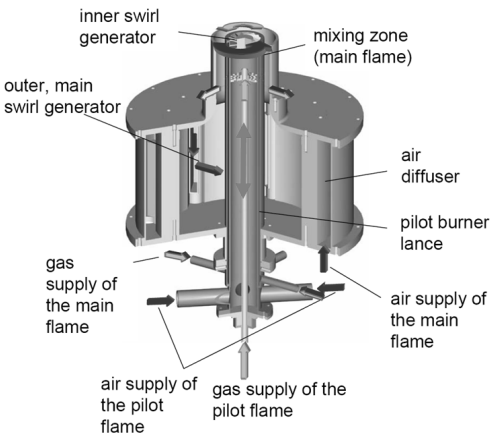

Fig. 2.1 Sketch of the double-concentric swirl burner with a central pilot burner [4]

The inner diameter of the main burner nozzle is $D_0 = 110mm$ and the outer diameter of the pilot burner is $d_0 = 70mm$. For isothermal investigations, the inner and outer flows were fed with air from a compressor, the measurements with swirl flames were carried out with premixed or non-premixed natural gas/air mixtures.
The normalized momentum flux ratio representing theoretical swirl number $S_{0,th}$ at the burner's exit is given in equation 2.1 with the tangential momentum flux $\dot{D}$, the axial momentum flux $\dot{i}_{ax,0}$ and the burner's exit radius R_0.

$$S_{0,th} = \frac{\dot{D}}{\dot{i}_{ax,0} \times R_0} \tag{2.1}$$

The swirl of the pilot flame was generated by an axial swirl generator with vanes and a theoretical swirl number $S_{0,th,pilot} = 0.79$ (equation 2.1). The main flow was swirled by tangential swirl generators with a theoretical swirl number $S_{0,th,main} = 0.90$. The axial pilot burner position with respect to the main burner outlet is the variable geometric parameter. In figure 2.1, the pilot burner outlet is aligned to the burner outlet ($x_{pilot} = 0mm$). The position of the inner pilot burner can be set up to 40 mm behind the burner outlet ($x_{pilot} = -40mm$).
The microphone probe was positioned at a fixed measurement position with a radial distance to the center line $r/D_0 = 4.55$ and an axial distance to the burner outlet of $x/D_0 = 1.0$, after having proven the independence of the noise measurements from the probe position due to the spherical noise emission characteristics [17].
Figure 2.2 shows the experimental setup for the investigations under enclosed conditions. The combustion chamber was designed with an optical access to investigate the flow fields of enclosed isothermal swirl flows and enclosed premixed swirl flames. With the microphone probe the flow and flame noise was detected to characterize the spectral and integral distribution of the noise from isothermal flows and combustion noise of swirl flames under premixed and non-premixed conditions.

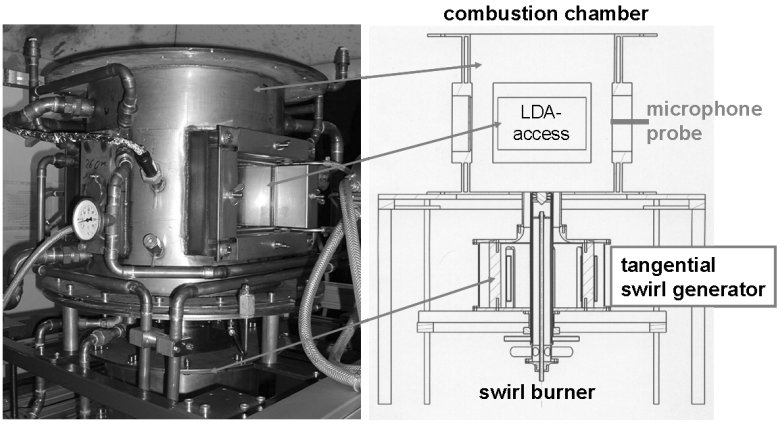

Fig. 2.2 Experimental setup to investigate enclosed swirl flows and swirl flames

2.2.2 Numerical Methods

2.2.2.1 Governing Equations

Basics of the numerical modelling are the compressible Favre-averaged Navier-Stokes equations and the energy equation; within the LES-formulation these read:

$$\frac{\partial \bar{\rho}}{\partial t} + \frac{\partial \bar{\rho}\widetilde{u}_i}{\partial x_i} = 0 \tag{2.2}$$

$$\frac{\partial \bar{\rho}\widetilde{u}_i}{\partial t} + \frac{\partial \bar{\rho}\widetilde{u}_i\widetilde{u}_j}{\partial x_j} = -\frac{\partial \bar{p}}{\partial x_i} + \frac{\partial(\widetilde{\tau}_{ij} - \tau_{ij}^{sgs})}{\partial x_j}. \tag{2.3}$$

$$\frac{\partial \bar{\rho}\widetilde{E}}{\partial t} + \frac{(\partial \bar{\rho}\widetilde{E} + \bar{p})\widetilde{u}_j}{\partial x_j} = \frac{\partial}{\partial x_j}(\widetilde{u}_j + \bar{q}_j - H_i^{sgs} + \sigma_{ij}^{sgs}) \tag{2.4}$$

where overbars and tildes denote the space-filtered and Favre-averaged scales. τ_{ij} and q_j are the viscous stress tensor and heat flux, respectively. τ_{ij}^{sgs} is the subgrid scale (sgs) stress tensor which is defined as $\tau_{ij}^{sgs} = \overline{u_i u_j} - \bar{u}_i\bar{u}_j$. Using the Smagorinsky subgrid Model [31], τ_{ij}^{sgs} is modeled as

$$\tau_{ij}^{sgs} = -2\rho\nu_t\bar{S}_{ij} = -\rho\nu_t(\frac{\partial \bar{u}_i}{\partial x_j} + \frac{\partial \bar{u}_j}{\partial x_i}), \quad \nu_t = (C_S\Delta)^2|\bar{S}_{ij}|, \tag{2.5}$$

where S_{ij} is the shear strain rate and C_S a model constant, it takes the value between 0.065 and 0.24 [15] dependent on the flow cases. In our case, $C_s = 0.1$ is used. The sgs enthalpy flux H_j^{sgs} is modeled similarly using a gradient transport model and the sgs viscous work term σ_{ij}^{sgs} is neglected.

2.2.2.2 The TFC Model

The turbulent flame speed closure (TFC) model [29, 33] was used for the combustion modeling. An addtional transport equation for the progress variable θ is solved in this model, which describes chemical reaction progress. θ is linearly related to the fuel or product mass fraction and has the value 0 in the unburned mixture and 1 in the burned mixture. In the framework of LES the transport equation of θ yields the form:

$$\frac{\partial \bar{\rho}\widetilde{\theta}}{\partial t} + \nabla \bullet (\bar{\rho}\widetilde{\mathbf{u}}\widetilde{\theta}) = \nabla \bullet (\frac{\mu_t}{Sc_t}\nabla\widetilde{\theta}) + \bar{\rho}_u S_t \left|\nabla\widetilde{\theta}\right|. \tag{2.6}$$

The turbulent flame speed S_t is an important parameter which covers the chemical/physical characteristics of the combustable mixture and the characteristics of the turbulent flow, it describes further more the interaction between turbulence and chemical reactions. The closure of equation (2.6) requires that S_t has to be expressed

via known values. Schmid [29] has theoretically derived an expression for S_t:

$$\frac{S_t}{S_l} = 1 + \frac{u'}{S_l}\left(1 + Da^{-2}\right)^{-1/4}, \quad Da^{-1} = \frac{\tau_c}{\tau_t} = \frac{\delta_F u'}{S_l L_t} = \frac{a u'}{S_l^2 L_t}. \tag{2.7}$$

u' is the velocity fluctuation and a the thermal diffusivity. L_t is the turbulent length scale quantified by $\Delta = C_S(\Delta_x\Delta_y\Delta_z)^{1/3}$; the turbulent velocity at subgrid scale is assumed as:

$$u'_\Delta = \frac{\nu_t}{\Delta} = C_S \Delta \sqrt{2\tilde{S}_{ij}\tilde{S}_{ij}}. \tag{2.8}$$

Other expressions for u'_Δ and Δ are possible and the reader is referred to [13, 15]. It has to be noted that u'_Δ is now grid dependent as well as the time resolved velocity. In the case of very small grid size $\Delta \to 0$, the filtered Navier-Stokes equations will switch to the exact unfiltered form. The turbulent diffusion terms in the filtered transport equations (equation 2.3, 2.4, 2.6) will vanish since $\mu_t \to 0$. The remaining term in S_t (equation 2.7) will be only the laminar flame speed S_l. In this case, the smallest eddies and the laminar flame front are resolved on the fine mesh and no modelling is needed. This makes a consistent transfer from LES to DNS.
S_l is the laminar burning speed and it describes the reaction solely from the mixture side. In premixed flames, the fuel is mixed with air in a certain ratio upstream of the burner, so that S_l can be given using a constant value. However, to solve flames with different air equivalence ratios λ, like the one in the current case (sec.2.2.2.4), the mixing effect of S_l has to be considered [29]. On the left side of figure 2.3, the dependency of S_l on the air equivalence ration λ is shown, the measured laminar flame speed [34] was fitted using the least-square-method via a fourth order ploynomial.
This TFC combustion model has been implemented in the commercial CFD code ANSYS CFX which uses an unstructured finite volume method (FVM) to solve the compressible Navier Stokes equations and is capable to run LES. The central difference scheme in space and 2nd order fully implicit time progress were used. Since the aim of the model is primarily to describe heat release, an integral one-step reaction $CH_4 + 2O_2 \to CO_2 + 2H_2O$ has been considered adequate for modelling methane/air

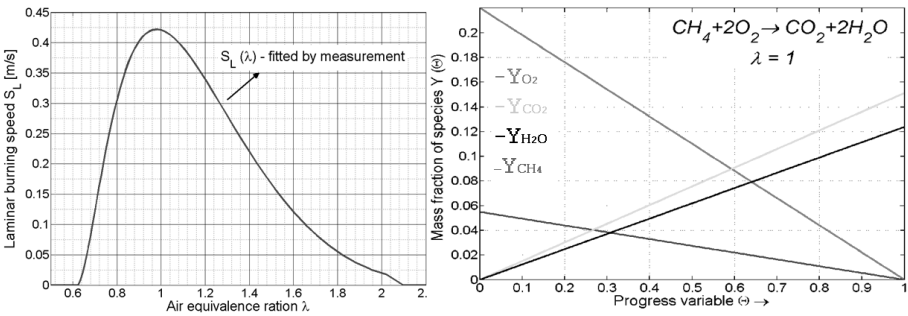

Fig. 2.3 Laminar flame speed S_L dependent on the air equalence ratio (left) and mass fractions over progress varialbe (right)

combustion. In this case, the reactants are completely burned to the stable product and all species concentrations are related to the progress variable θ via simple algebraic equations. On the right hand side of figure 2.3 the relations between the species mass fractions Y_i and the progress varible Θ for the stoichiometric mixture case is shown. The product concentrations (Y_{H_2O} and Y_{CO_2}) increase linearly with Θ, whereas the fuel concentration Y_{CH_4} straightly falls.

2.2.2.3 Lighthill's Acoustic Analogy

The Lighthill's acoustic equation for the density fluctuation results by conversion of the basic fluid mechanics equations without any approximation and linearization [24]:

$$\frac{\partial^2 \rho'}{\partial t^2} - c_0^2 \Delta \rho' = \frac{\partial^2 T_{ij}}{\partial x_i \partial x_j}, \tag{2.9}$$

$$T_{ij} = \rho v_i v_j - \tau_{ij} + \delta_{ij}(p' - c_0^2 \rho'). \tag{2.10}$$

T_{ij} is the Lighthill's stress tensor and c_0 the sonic speed. The left hand side of equation 2.9 has the form of a linear wave equation and the right hand side of this inhomogeneous wave equation can be considered as a source term presuming no viscous terms and small Mach numbers. While the turbulent reacting flow acts as a source, the acoustic waves propagate in a uniform acoustic medium. The transfer of informations from the sources to the external medium is achieved through the Lighthill stress tensor T_{ij}. In a turbulent reacting flow, the viscous stress τ_{ij} in T_{ij} is very small in comparison to the other terms and can be neglected. The velocity correlation term $\rho v_i v_j$ (Reynolds-stress term) and $p' - c_0^2 \rho'$ represent the sources caused by the turbulent flow and by the unsteady heat release. An order of magnitude analysis of the Lighthill's tensor showed [11] that the ratio of both terms scales to Ma^2, which indicates further, that for turbulent reacting flows at low Mach numbers $Ma^2 << 1$, the dominant term will be the last one on the right hand side of equation 2.10. Another version of the Lighthill's equation can be derived for the pressure fluctuation p' in the same way [24]:

$$\frac{1}{c_0^2} \frac{\partial^2 p'}{\partial t^2} - \Delta p' = \frac{\partial^2 T_{ij}^*}{\partial x_i \partial x_j} + \frac{\partial^2 W}{\partial t^2}, \tag{2.11}$$

$$T_{ij}^* = \rho v_i v_j - \tau_{ij}, \quad W = \frac{1}{c_0^2} p' - \rho'. \tag{2.12}$$

$\frac{\partial^2}{\partial x_i \partial x_j} T_{ij}^*$ and $\frac{\partial^2}{\partial t^2} W$ are then the sources responsible for the generation of pressure fluctuations.

2.2.2.4 Numerical Setup

The combustable mixture consists of fully-premixed air/natural gas. For the numerical simulation, the total thermal load of both flows is 135 kW, the important operational parameters are listed in table 2.1. $\dot{V}$ is the volume flow rate, λ the air equivalence ratio and S the theoretical swirl intensity.
Figure 2.4 shows the simulation domain and mesh of the open swirled flame with

Table 2.1 Operational parameters in the experiment

$\dot{V}_{main}$	$180 m_N^3/h$	λ_{main}	1.5	S_{main}	0.9
$\dot{V}_{pilot}$	$20 m_N^3/h$	λ_{pilot}	1.05	S_{pilot}	0.79

a planar pilot lance. The considered computational mesh represents the main parts of the interior flow domain of the burner and a large free domain downstream of the burner exit where reaction takes place. The axial swirl generator in the pilot flow was also included in the computational mesh. A block-structured grid with about 50 blocks and 1 mio. nodes was used. A time step of $10\mu s$ was chosen to keep the Courant-number. smaller than one. Colors of the planes denote types of the boundary conditions, which were set according to tab.2.1. The static pressure or total pressure (depending on the flow direction) and the temperature values are fixed like for the ambient air at the opening boundaries. No slip walls with constant temperature have been used for burner walls. The Reynolds-number based on the nozzle axial velocity and diameter of the main flow was Re $\approx$ 27000. The pilot lance can be retracted by 40mm as clearly shown in figure 2.5.

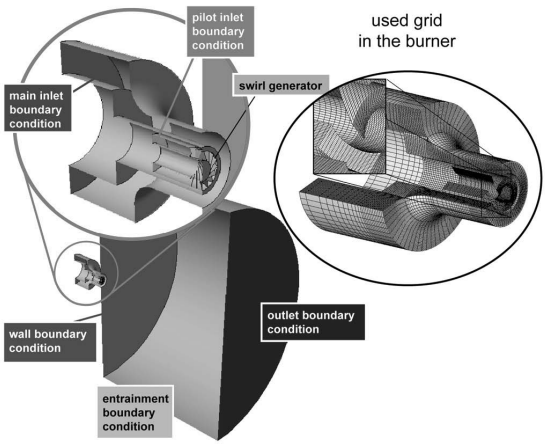

Fig. 2.4 Flow domain and mesh used in the simulation

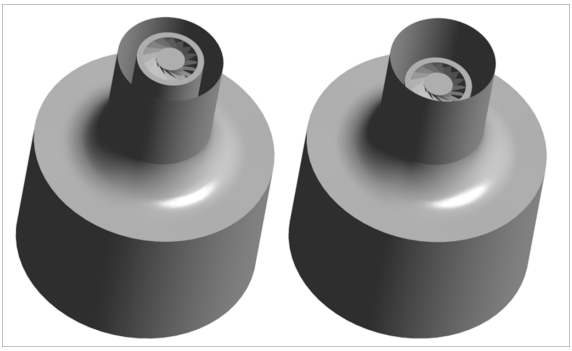

Fig. 2.5 Swirl burner with a planar (left) and a recessed (right) pilot lance

2.3 Results and Analysis

2.3.1 Experiment

2.3.1.1 Acoustic Characterization of Isothermal Swirl Flows

In the following section the results of experimental investigations of the isothermal, turbulent flow field of the new burner design are presented. The experiments were carried out under variation of the main operation and geometrical parameters like swirl intensity, flow rate and burner outlet geometry (axial position of the pilot burner). In figure 2.6 the results of the time-averaged isothermal flow field at four planes in the vicinity of the burner are plotted. The theoretical swirl number of the main and pilot flow are $S_{0,th,main} = 0.90$ and $S_{0,th,pilot} = 0.79$ and the axial position of the pilot burner is $x_{pilot} = 0mm$. The profiles of the axial velocity, starting nearby the burner outlet ($x/D_0 = 0.05$, cross) with the divided pilot and main flows, are shown. With increasing distance to the burner outlet the typical behavior of a strongly swirling flow was observed: The separation of the pilot and main flow disappears, indicating the fast mixture of the two flow fields, and at the centre line

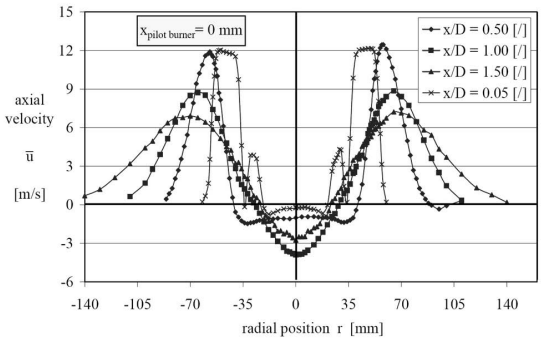

Fig. 2.6 Axial velocity profiles of the isothermal flow at four planes [4]

a inner recirculation zone with negative axial velocity (opposite to the main flow direction) can be identified.
The remaining single swirling jet spreads radially and, caused by the free flow field, entrains surrounding, non-rotating medium, while propagating further downstream ($x/D_0 = 0.50, 1.00, 1.50$). Measurements of the noise emissions of the isothermal swirl flow showed values of the sound pressure level $SPL = 20 \times log(\frac{p_{rms}}{p_{0,rms}}) = 75.7dB$ ($x_{pilot} = 0mm$, $p_{0,rms} = 2 \times 10^{-5} Pa_{rms}$) at the fixed measurement position with a radial distance to the center line $r/D_0 = 4.55$ and an axial distance to the burner outlet of $x/D_0 = 1.0$. An interesting result is the negligible influence of the swirl intensity and the strong influence of the flow rate (burner outlet velocity) on the turbulent flow noise. The value of 75 dB at a volume flow rate of $\dot{V}_{n,air} = 200 m_N^3/s$ and the described measurement position is the minimal order of magnitude which cannot be undercut for the used isothermal, turbulent swirl flow.

2.3.1.2 Periodical Flow Instabilities in Isothermal Swirl Flows

To investigate the dynamic behaviour of the emitted noise more detailed, the acquired data from the microphone probe ($r/D_0 = 4.55$, $x/D_0 = 1.0$) were analysed in the frequency domain to get more information of the spectral distribution of the sound pressure ratio. Referring to the first burner configuration (see chapter 2.3.1.1) the pilot burners outlet was aligned to the burner outlet ($x_{pilot} = 0mm$) and the spectral distribution shows the typical behaviour of the turbulent disturbances in an isothermal, turbulent flow field (figure 2.7 dashed blue line; [4, 18]). In figure 2.7 the distribution of the emitted sound pressure is shown with the pilot burner drawn back 40 mm upstream the burner outlet (black line). Industrial burner applications with lean-premixed flames often use recessed components like pilot burners and bluff-bodies to prevent thermal damage of the sensitive units, examples are Siemens V64 [20] and Pratt & Whitney FT 8 [12]. The spectral distribution of the sound pressure shows a dominating peak at a frequency f = 56 Hz. In comparison to the aligned

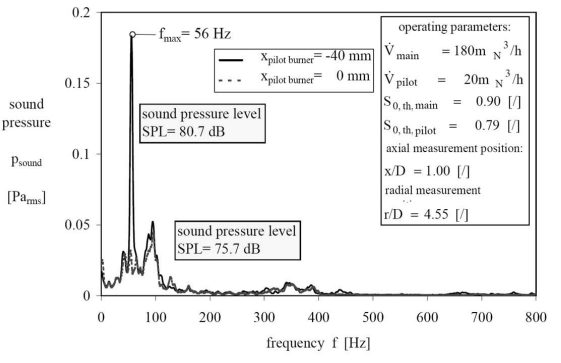

Fig. 2.7 Spectral distribution of the sound pressure of an isothermal swirl flow with different positions of the central pilot burner ($x_{pilot} = 0mm / -40mm$)

pilot burner $x_{pilot} = 0mm$ the peak increases the total SPL from 75.7 dB to a level of 80.5 dB. The influence on the acoustic field was identified as a consequence of periodic oscillations of the axial position of the inner recirculation zone in the swirl flow and the quantified increase of the sound pressure level is caused by a periodic disturbance of the isothermal flow field, shown by spectral distributed measurements of the flow field. The underlying physical mechanism is described by [10, 18] and shows a time-dependent axial movement of the recirculation zone, causing a time-dependent effective swirl number $S_{eff} = S_{eff}(t)$ and the stabilization point of the recirculation zone changes the different positions sinusoidally.
The variable burner design enables to generate periodical flow disturbances in an isothermal swirl flow. The consequence for further burner constructions is the need to prevent coherent flow structures caused e.g. by recessed pilot burner constructions, as often used in common industrial burner designs [12, 20].

2.3.1.3 Premixed Swirl Flames

Noise Sources in premixed Swirl Flames: Influence of Operating Parameters

In figure 2.8 the results of sound pressure measurements of premixed swirl flames are presented. The experiments were carried out with a constant pilot flame of a thermal load $\dot{Q}_{th,pilot} = 20kW$ and an air equivalence ratio of $\lambda_{pilot} = 1.05$ to guarantee a stable pilot flame. The pilot burner is positioned at the level of the burner outlet ($x_{pilot} = 0mm$). It is obvious, that the thermal output of the premixed main flame increases the sound pressure considerably. The reacting flow shows a sound pressure level of about 25 dB higher than the SPL of the isothermal flow (gas flow rate substituted by air). This part is called flame-induced noise and is caused by the volume expansion and density fluctuations in the flame due to the massive increase of the exhaust gas temperature. A two times enhanced thermal output of the main flame ($\dot{Q}_{th,main} = 150kW$ *and* $300kW$) causes an increase of the SPL from 103 dB to nearly 108.5 dB, whereas the influence of the air equivalence ratio λ_{main} is negli-

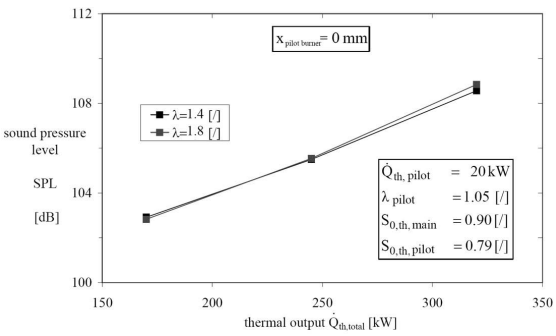

Fig. 2.8 Sound pressure level of premixed flames under variation of thermal load and air equivalence ratio main of the main flame

gible (see figure 2.8).

Noise Sources in premixed Swirl Flames: Variation of Geometric Parameters

Next, the influence on the noise of premixed swirl flames of the geometric parameters was investigated. For isothermal flows the influence was predominant (see chapter 2.3.1.2) and the question to be answered was how do premixed flames react on such disturbances of the flow field. In figure 2.9 the dependency of the burner outlet geometry on the sound pressure of premixed flames is presented. The spectral distribution is almost identical for all frequencies except f = 101 Hz. The recessed pilot burner generates dynamic, periodic structures in the flow field. It should be pointed out that the existence is not limited to isothermal flows. Corresponding to that fact such structures influence the investigated flames and their formation and combustion lead to an increase of the SPL of 2.3 dB (+30%).
Comparing reacting and isothermal cases shows that in the isothermal flow the frequency of the periodic disturbance is lower. The frequency distribution of flames covers a wider frequency band. The Strouhal number Str ($= f_{peak} \times D_0/u_0$) for both cases reveals the same values (0.74 (premixed flame) and 0.72 (isothermal flow)). This proves that the effect is originated from the same physical phenomenon [18]. In figure 2.10 the results for identical combustion parameters with variation of the burners exit geometry are plotted. The varied pilot burner position influences the sound pressure level of the flame in the same way as in the isothermal case. The recessed pilot burner $x_{pilot} = -40mm$ generates coherent structures in the flow field and, therefore, the SPL increases in the presented case about 2.5 dB (+33.5%).

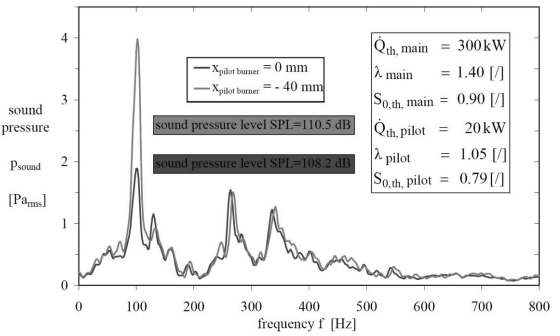

Fig. 2.9 Spectral distribution of the sound pressure of premixed flames with different burner exit geometries (different positions of the pilot burner $x_{pilot} = 0mm,\ and\ -40mm$)

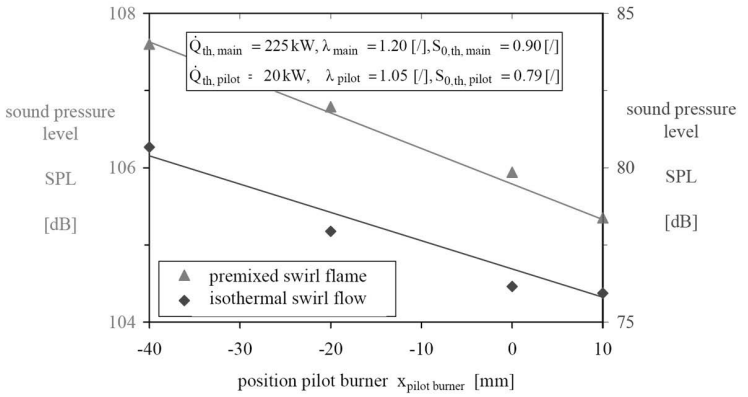

Fig. 2.10 Influence of the pilot burner position x_{pilot} on the sound pressure level of premixed swirl flames

2.3.1.4 Noise Sources in Non-Premixed Swirl Flames

In the second part of the characterization and quantification of noise from reacting flows non-premixed flames were studied and results were compared to investigations of premixed flames, which were carried out to get a classification of all technically relevant type of flames. The difference to the above described premixed flames is the location and the way of gas injection. In the case of premixed flames a mixture of fuel and air leaves the burner exit, whereas the air equivalence ratio is constant across the burner outlet area. For non-premixed flames the burner outflow consists of pure air, the gas is injected directly into the flame zone. This leads to a mixture of fuel, air and hot combustion products in the flame zone with the effect of fuel-rich and fuel-lean regions and the effect that the flames are often longer than premixed flames of same operating parameters, caused by a time delay for mixture formation before ignition occurs. Consequently, a lower volumetric reaction density is characteristic for non-premixed flames, which causes disadvantages like higher, local temperatures (NOx-formation) and soot formation.

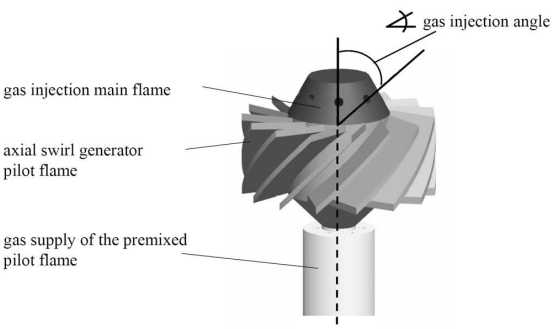

Fig. 2.11 Sketch of the gas injection for non-premixed flames

Variations of Geometric Parameters

The investigations of non-premixed flames were carried out with the same double-concentric swirl burner configuration, mentioned before. The gas injection was located at the central bluff-body of the pilot burner and the parameter to influence the flame characteristics (type-I- / type-II-flame) is the gas injection angle to generate technically relevant flames for different applications like jet engines or industrial furnaces. The angle (see figure 2.11) is defined between the direction of the gas flow and the burner axis. Figure 2.12 shows the realization of different types of non-premixed flames by varying the gas injection angles in a range of 0^o to 90^o in steps of 15^o. Figure 2.13 shows the results for variation of gas injection angles between

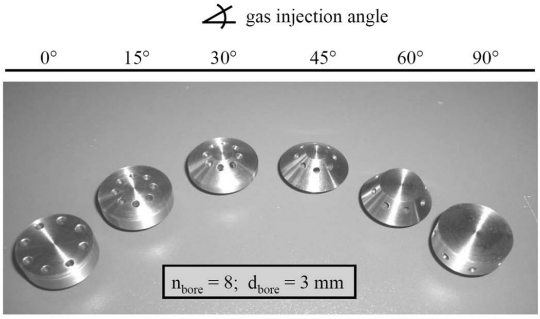

Fig. 2.12 Gas injection nozzles to realize different types of non-premixed flames

30^o and 90^o with variation of the air equivalence ratio. A decrease of air equivalence ratio should induce an increase of sound pressure level. But non-premixed flames show a remarkable behaviour: The sound pressure level is almost constant at SPL between 104 dB and 108 dB. It could be observed, that the non-premixed flames are partly louder than the equivalent premixed flame, which introduced the question whether there are other physical mechanisms influencing the combustion noise. A difference between the operating conditions of premixed and non-premixed flames is the existence of the pilot flame. The non-premixed flames have one central fuel

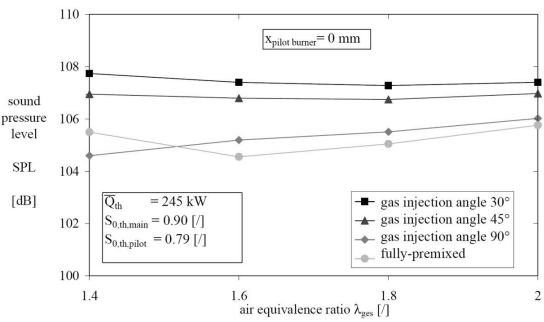

Fig. 2.13 Sound pressure level of non-premixed flames under variation of air equivalence ratio λ_{main} and the gas injection angle

supply and the different gas injection angles effect different stabilization points of the different flames. The next consequent step was the prevention of these fluctuations of the stabilization point by use of a premixed pilot flame.

Variation of Flame Stabilization: Influence of Pilot Flame

To investigate the influence of main flame stabilization by a premixed pilot flame, the same thermal load and the air equivalence ratio of the pilot flame as adjusted for investigations under premixed conditions of pilot and main flame were used. This enables to compare the premixed and non-premixed main flames with a stable, stationary ignition point of the main flame. The investigations showed the need of a locally stable ignition for investigations of the combustion noise, because the fluctuation of the flame ignition point causes an increase of noise up to 5 dB. But for such conditions a comparison with premixed flame cannot be done. Applying the premixed pilot flame in all cases, the non-premixed flames are always more quiet than the comparable premixed flame, which can be explained by lower reaction density of the non-premixed flames.

The experiment showed two regimes of non-premixed flames (figure 2.14): Louder

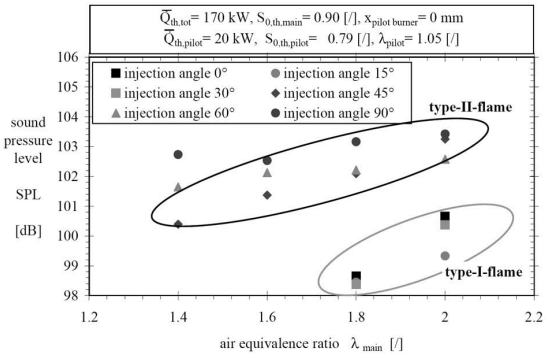

Fig. 2.14 Sound pressure level of non-premixed flames with premixed pilot flame under variation of air equivalence ratio λ_{main} and the gas injection angle

flames have an injection angle between 45^o and 90^o and look like premixed flames (blue, short flame zone) and the SPL is with values of 101-103 dB very close to premixed flames (SPL = 103-105 dB). The loudest non-premixed flames are the flames of a gas injection angle of 90^o, leading to almost the combustion noise of fully-premixed flames (figure 2.15). The second regime with the smaller injection angles ($0 - 45^o$) is characterized by long, soot-forming flames with very low volumetric reaction densities. The SPL of this regime is very low at values of 96-100 dB (dependent from air equivalence ratio λ).

With the stable and time-independent ignition point of the non-premixed flame a possibility is shown to compare different types of non-premixed flames and to com-

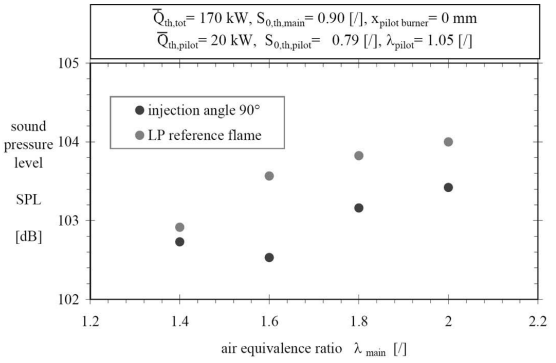

Fig. 2.15 Comparison of the sound pressure level of a premixed and non-premixed swirl flame

pare results with experiments for premixed operating conditions and another physical mechanism of noise generation especially under non-premixed conditions was detected and can be separated from the other noise sources.

2.3.1.5 Enclosed Premixed Swirl Flames

The test facility consists of the double-concentric swirl burner (figure 2.1) and a combustion chamber with an inner diameter $D_{cc} = 0.44$ m and a length l_{cc}= 0.5 m (figure 2.2). Figure 2.16 shows the dependence of the sound pressure level of combustion noise - measured at the wall of the combustion chamber (axial position $x_{microphone} = 0.25m$) - from the thermal load of the flame and the air equivalence ratio of the main flame (see chapter 2.2.1). The results showed that the operating parameters of the flames are limited, caused by the tendency of lean-premixed flames to get self-sustained combustion instabilities, being an order of magnitude louder than the stationary flames. In figure 2.17 the characteristics of a stationary and an oscillating flame are compared and the difference which is limited to the increase of

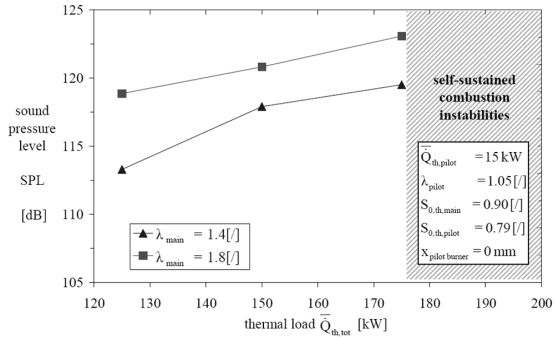

Fig. 2.16 Combustion noise of enclosed, premixed swirl flames

one preferential frequency - leading to an increase of the SPL of more than 6 dB - is obvious.

The investigations were made for a stationary operating point to compare results

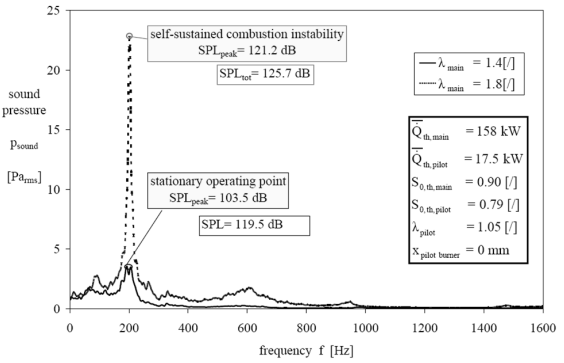

Fig. 2.17 Boundary between combustion noise and self-sustained combustion instabilities

with non-enclosed premixed flames (see chapter 2.3.1.3). The most important result is the level of the combustion noise in the chamber which is up to 20 dB louder caused by reflection of noise at the combustion chamber's wall and the higher level of temperature in the chamber with the formation of outer recirculation zones.

2.3.2 Numerical Simulation

2.3.2.1 Isothermal Flow

The simulations shown in the current section cover both the isothermal flow and the reacting flow with premixed flames. The x-axis is defined as the streamwise direction and $x = 0$ denotes the outlet plane of the annular main flow. In figure 2.18 the measured data and the results from the simulation are drawn. This gives an overview of the isothermal flow field displaying the time averaged radial profiles of the streamwise velocity component at four axial positions in the vicinity of the burner (x/D_0=0.05, 0.5, 1.0 and 1.5). The straight line shows the time averaged results of LES and the circles denote the measured data. On the axis a central, inner recirculation zone (IRZ) with the corresponding negative values for the axial velocity can be identified. The comparion shows very good agreement for both methods.

2.3.2.2 Dynamic Structures in the Isothermal Flow

To look more into details of the dynamic behavior of the isothermal flow, sound pressure data acquired with a microphone probe in the ambient of the swirling flow,

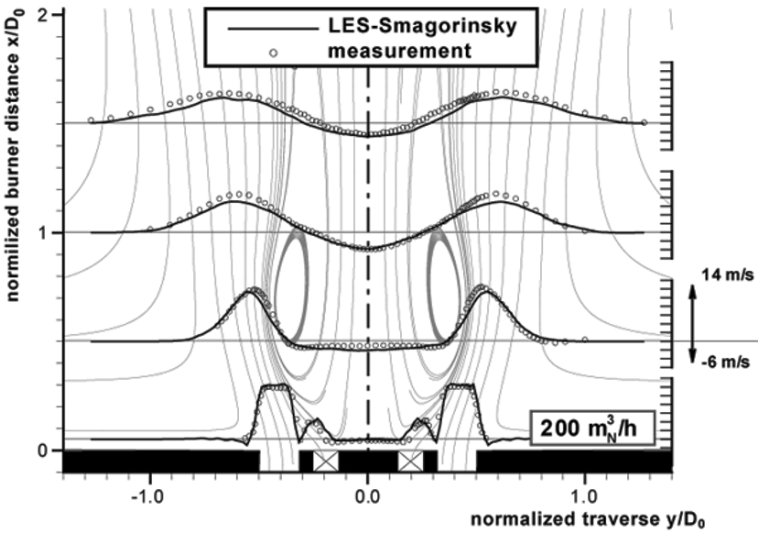

Fig. 2.18 Comparison of calculated mean streamwise velocity profiles with measurement at several axial positions in the isothermal flow case [18]

were analyzed with respect to their spectral representation. As clearly demonstrated in figure 2.19, the formation of periodic coherent structures (red line) in dependence of the chosen burner outlet geometry ($x_{lance} = -40mm$) does not effect the shape of the sound level spectra at all, but adds a considerable contribution at 56 Hz, resulting in an increase of the sound pressure level (SPL) from 75.7 dB to 80.7 dB. Figure 2.20 shows results of another LES calculation using the same computational

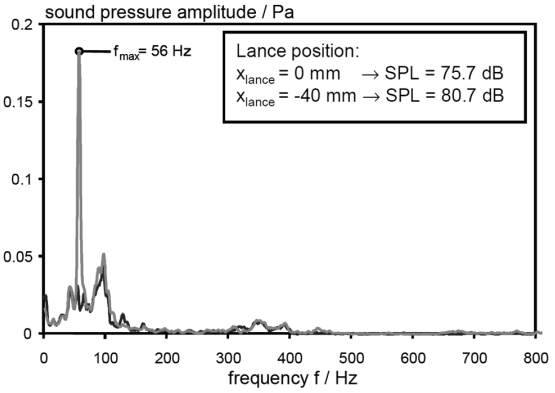

Fig. 2.19 Measured spectral distribution of sound pressure amplitudes and wavelength-integral sound pressure levels for two lance positions in the isothermal swirling flow. Blue line: $x_{lance} = 0mm$; red line: $x_{lance} = -40mm$ ($\dot{V}_{main} = 190m_N^3/h$, $\dot{V}_{pilot} = 10m_N^3/h$, probe position: $x/D_0 = 1$, $y/D_0 = 4.55$)

solution procedure, but utilizing a total volume flow of $\dot{V}_{main} = 650m_N^3/h$, where a spectral representation of the calculated static pressure at a monitoring point in the ambient flow is compared to an according measured normalized sound pressure

level. The experiments are not directly comparable, as they were performed utilizing only $\dot{V}_{main} = 609 m_N^3/h$, which turned out to be the maximum inflow, that could be supplied by the compressor. Anyhow, the observed preferential frequencies compare very well. This indicates that the coherent structures result from an axial displacement of the central recirculation zone, which is characteristic for swirl flows. This supports the mechanism for the generation of coherent structures in swirl flames as already mentioned above and earlier found in literature ([10]).

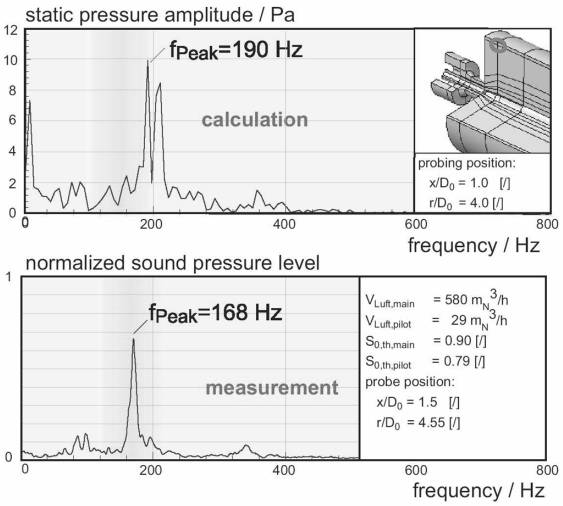

Fig. 2.20 Comparison of spectral resolved static pressure amplitude and normalized sound pressure level in the ambient flow of the isothermal swirling flow

2.3.2.3 Reating k with Premixed Flames

The LES-calculation of the swirled flame was run for about 20.000 time steps ($\approx$ 0.2s). Figure 2.21 shows comparisons of the mean streamwise and tangential velocity profiles between measured data and LES results at two axial positions: $x/D_0 = 0.05$ and $x/D_0 = 0.5$. Since the flow field is charged with very strong swirl, the inner recirculation zone (IRZ) can also be detected in the premixed flame case. The results of both LES/Exp. are qualitative in good agreement. The plane $x/D_0 = 0.05$ lies 5mm above the burner exit, at this positions, sharp gradient of the velocity components forms, as the cold mixture penetrates into the steady ambience. Further downstream, due to the strong viscosity generated by the turbulent flow, the gradient becomes smoother. In the middle of the top right figure, the backflow can be detected again by the negative axial velocity. However, there is a difference directly above the pilot lance for the mean axial velocity, which was overpredicted in the simulation. This may be caused by the main inlet boundary condition, where the rotational velocity was not exactly known. The used relative coarse grid (1 mio. cells) may be an other reason. Also, uncertainties like definitions of the sub grid

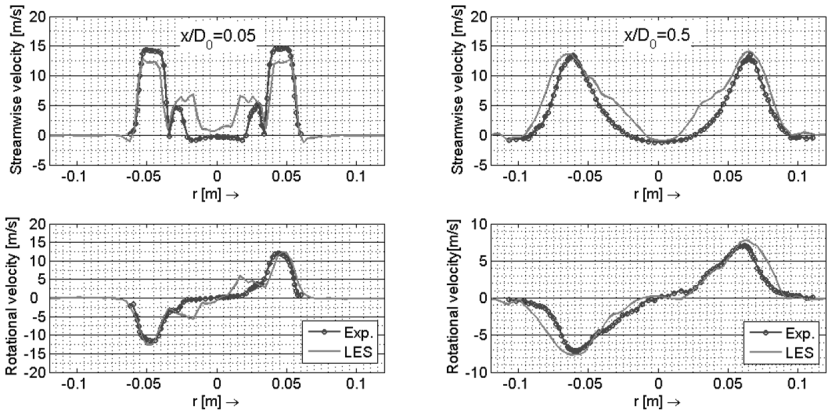

Fig. 2.21 Comparison of the mean velocities between LES and measurement

scale turbulent fluctuaions u'_Δ and the turbulent length scale Δ (see sec.2.2.2.2), or the use of a constant C_S remain still in the model. Nevertheless, similar problems can also be found in other literatures [30, 32, 14, 26], particularly for swirled flame in the vicinity of the burner exit. In figure 2.22, iso-surfaces of the vorticity $|\omega| = |rot \times \mathbf{u}| = 4000s^{-1}$ are shown together with contours of a slice at $x/D_0 = 3$. As expected, the local vortex tubes showed a helical structure and the iso-contours on the slice have also an annular form.

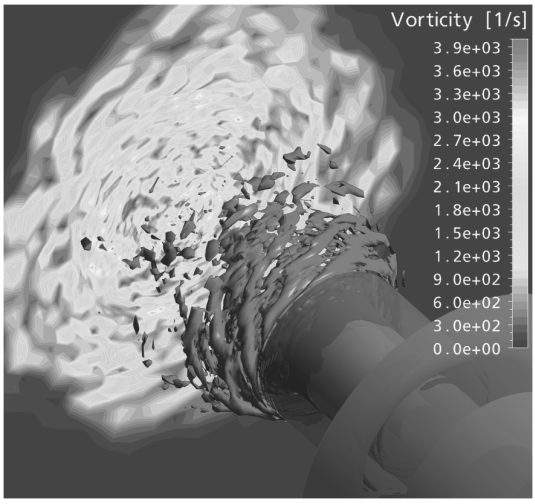

Fig. 2.22 Iso-surfaces of the vorticity $|\omega| = 4000s^{-1}$ and an axial slice of vorticity at $x/D_0 = 3$

2.3.2.4 Flame Dynamics

Figure 2.23 shows slices of the instantaneous progress variable and temperature for the open flame case with planar lance. The progress variable increases immediately from zero to one at the reaction zones where the cold mixture reacts to the hot products. At the same time, as the inner flow reaches the outlet of the burner, strong turbulence is generated due to the huge expansion of flow field, vortices shed from the burner mouth. Accordingly, the flame front becomes corrugated by the local turbulence. One notes, that the pilot flow has an air equivalence ratio of 1.05 (see sec.2.2.2.4, tab.2.1), which is very close to the stoichiometric mixture of methane and air. As a result, areas with the highest temperature are located near the burner axis directly above the pilot lance, the shape of this region is affected by the IRZ and the main jet. The IRZ causes a recirculation of the hot gases back to the reaction zones and supports the ignition stability of the flame. That is the main benefit of using swirled flows. Another reason is is that more intensive heat release can be achieved due to the high turbulence intensity. In figure 2.24, the instantaneous

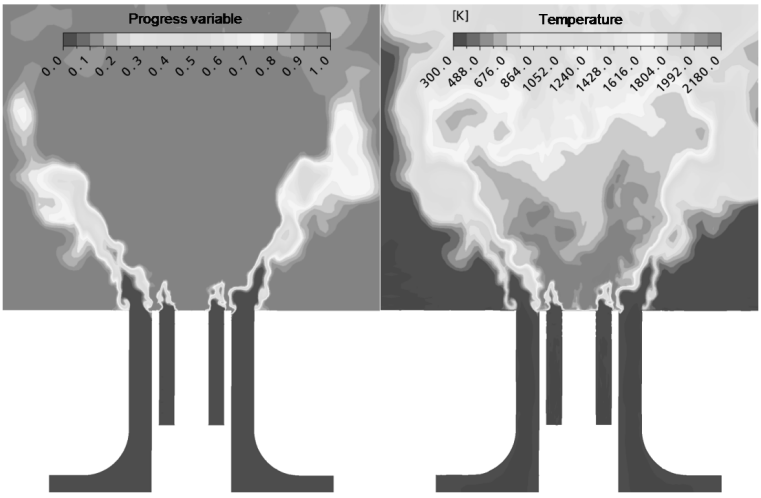

Fig. 2.23 Slices of the instantaneous progress variable (left) and the temperature (right)

contours of the sub grid scale turbulent fluctuations $u'_\Delta = C_S \Delta |\tilde{S}_{ij}|$ (sec.2.2.2.2) are shown. These are particularly large at the reaction zone and the shear layers, because the shear strain rate S_{ij} is very high in these regions. The flow is strongly accelerated at the reaction zone due to the expansion effect. The black curves in figure 2.24 represent the iso-contour lines of a selected reaction rate for θ by $\dot{\omega} = 80 kg/m^3/s$. As can be seen, the flame front is stabilized by the IRZ at the corners at the exit of the burner mouth. As only small eddies are generated and shed from the burner, these will be completely burned up by passing through the flame front and make the flame front corrugated. Further downstream, as the turbulence becomes large scaled,

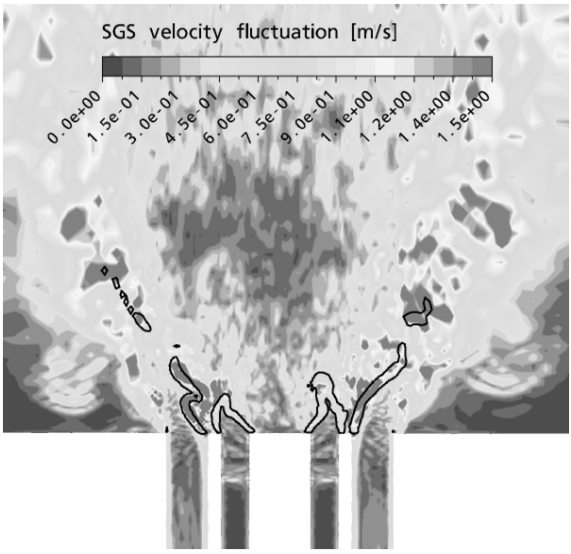

Fig. 2.24 Sub grid scale velocity fluctuations

these can not be completely burned by the flame front due to the higher fluctuations. The flame front is teared and small flame spots form in the burned gas. These can be detected by the isolated iso-contours in figure 2.24. In the context of the LES, the maximal resolvable flame thickness will be the local grid size Δ. The theoretical laminar flame front with about 0.1mm thickness can not be resolved on the coarse LES-grid. However, the TFC combustion model within the framework of LES filters implicitly the sharp gradients at the reaction zones through several LES-cells. In this case, the modeled eddies in the sub grid can penetrate into the flame and thicken the flame front. The resolved large eddies will then wrinkle and corrugate the flame. Thus, the simulated flames in our case are located in the thickend flame and corrugated flame regimes of the flame structure-diagram. On one hand, the assumption of the LES-modeling has caused this conclusion; and on the other hand, since the reacting flow has a very high Reynolds-number, a wide range of turbulent scales exists and therefore, there is turbulence with scales smaller than the laminar flame thickness.

2.3.2.5 Coherent Structures in Premixed Flame

In the case with a recessed pilot lance by -40 mm (figure 2.5), a coherent structure can be identified similar to the isothermal flow case (sec.2.3.2.2). This coherent structure has been identified and visualized using a phase locked averaging method in [19] for the isothermal flow case. As soon as the main flow reaches the exit plane of the pilot lance, the axial momentum of the main jet will decrease due to the expansion of the flow field. This causes the swirl instensity in this region to increase, so that the so formed IRZ can even overcome the combined inertial axial momentum

of the inner flow. As a result, the flow points into the direction of the burner where it acts as flow perturbance. However, as the IRZ moves into the burner mouth, the outlet area of the burner will be reduced and this causes a higher axial momentum. Consequently, the swirl intensity will drop and the IRZ moves again to the outside of the burner. The IRZ becomes unstable in this case and moves backwards and forwards to the burner periodically. This is the mechanism of the coherent structure formation and it causes a very high tonal peak frequency in the spectrum of the pressure fluctuations [4, 10]. In figure 2.25, two calculated typical meridian cuts of the streamwise velocity fields are shown. Both fields represent a time delay of $\Delta t = 2.7ms$. The black lines denote isolines of the axial velocity by $u = -1m/s$. In the first snap shot (at the left of figure 2.25), the IRZ flows towards the burner due to very high swirl intensity and there is a large region with negative axial velocity at the burner mouth. In the second image (on the right of figure 2.25), the IRZ moves outwards to the outside of the burner and no backflow is observed near the burner mouth. This makes one turnaround approximately 2x2.7ms (about 180Hz).

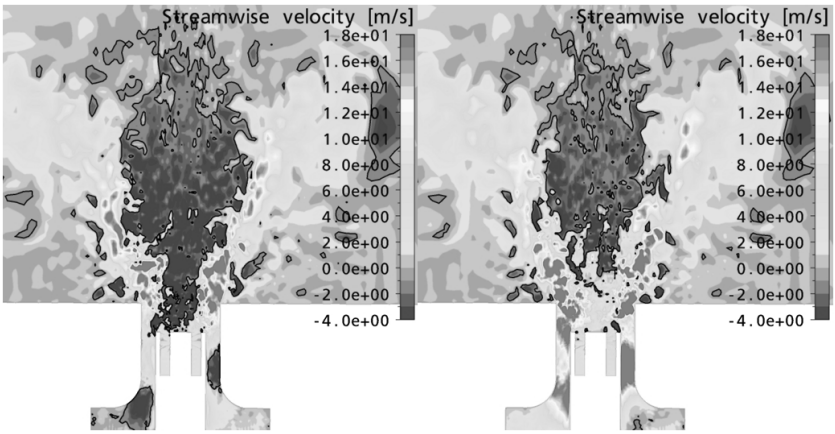

Fig. 2.25 Snap shots of the axial velocity near the burner mouth, black curves denote isolines by $u = -1m/s$

2.3.2.6 Analysis of the LES Result

In section 2.2.2.3 the acoustic analogy has been introduced and an order of magnitude analysis of the Lighthill tensor has been performed. In figure 2.26 and figure 2.27, the two major contributions to the Lighthill tensor are compared for the same point in time by a slice view. These are on the one hand the aeroacoustic source $S_{aero} = \frac{\partial^2}{\partial x_i \partial x_j}(\rho v_i v_j)$ and on the other hand the combustion noise source $S_{cn} = \frac{\partial^2}{\partial x_i \partial x_i}(p' - c_0^2 \rho')$, defined in equation 2.9 and equation 2.10. As can be seen, the main source regions are located close to the nozzle exit of the burner, where

the flow domain expands and combustion occurs. Due to very strong variation of the density, the combustion noise source is located solely at the thin reaction zones. Moreover, the expansion of the inflows into the free domain and the chemical reaction causes strong turbulence and acoustic sources were generated, which are evident from figure 2.26, where one can detect both the reaction zones and vortex structures along the jet flame. The magnitude of S_{cn} is about 3 order higher than the magnitude of S_{aero}. This is reasonable since the overall observed Mach numbers are smaller than 0.07 and $S_{aero}/S_{cn} \propto Ma^2$. In fact, for subsonic flow with large reynolds number, the combustion process causes much stronger density variation than the turbulent motions. It is noteworthy, that large values of the acoustic sources

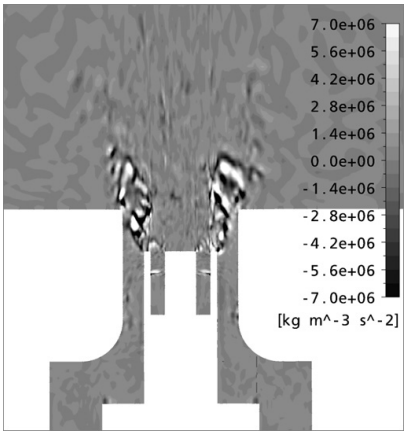

Fig. 2.26 Contour plot of the aerodynamic source S_{aero}.

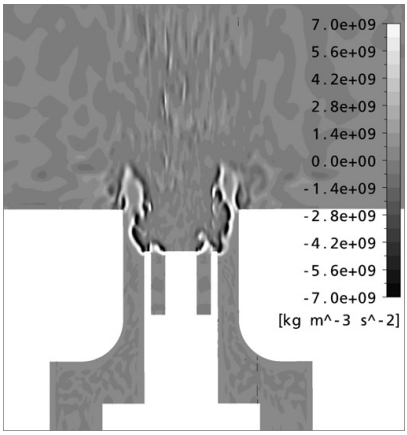

Fig. 2.27 Contour plot of the combustion noise source S_{cn}.

do not directly lead to higher noise level at farfield. However, these can be used as input data for other CAA methods (Computational Aero-Acoustics). Bui et al. [7, 8] have proposed the APE (Acoustic perturbation equations) to compute combustion generated noise using acoustic sources calculated by a LES simulation and found out, that the sound pressure level caused by the chemical reaction is significant larger than the one caused by the turbulent flow [7]. It is also proved by the acoustical measurements [4, 6], that the SPL of the reacting flow is much higher than the isothermal flow. Figure 2.28 gives an overview of the instantaneous vortex sound power according to Bamberger [2]

$$P_{vortex} = -\int \rho(\omega \times \mathbf{u})\mathbf{v_{ac}} dV, \tag{2.13}$$

with the density ρ, the vorticity ω, the acoustical velocity $\mathbf{v_{ac}}$. A positive net power delivers acoustic energy. As expected, the highest integrated vortex power are located along the shear layer of the jet. During the LES several monitor points (MP) in the flow domain have been used to follow the temporal progress of the flow vari-

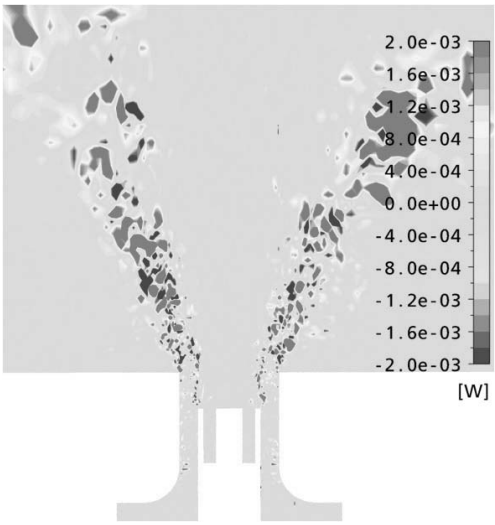

Fig. 2.28 Acoustic power of vortex given bei equation 2.13

ables. In figure 2.29, a frequency analysis of the monitor point (as indicated in the small slice) is made for the pressure und density fluctuations, this MP lies in the main annular flow. A distinct preferential frequency at 150Hz can be identified from the spectra of ρ' and p', which is known as the eigen frequency of the burner. In this case, the burner system acts as a Helmholtz-resonator due to the narrowed cross section in the annular main flow. The gas column in the burner throat works as inertial mass and oscillates via the gas volume, which acts as spring upstream in the burner. The corresponding flow structure will be transported downstream to the outside of the burner and can be detected in the main jet (figure 2.30). It also caused periodic fluctuation of the local mixture fraction in the reaction zone, and as a result, the reaction rate fluctuates with the same frequency.

In figure 2.30, a spectral analysis of the monitor point MP5 in the swirled jet (as indicated in the scmall slice) is shown, on the left, for ρ' and p'; and on the right, for

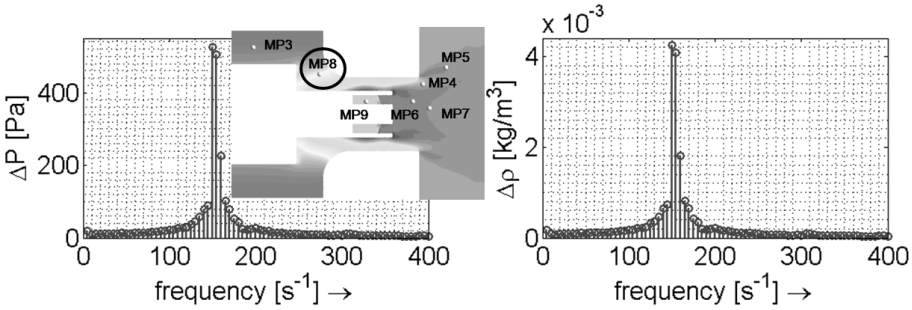

Fig. 2.29 Spectra of the monitor point MP8 in the burner inner flow.

the two main sources S_{aero} and S_{cn} in the Lighthill's equation for p' (2.11). Besides of the eigenfreqency of the burner, another dominant frequency at 180Hz arises in the spectra of ρ' and p' in the jet flame. This is caused by a coherent structure. The IRZ becomes unstable and moves in and out from the annular main flow periodically (sec.2.3.2.5). The mechanism of the coherent structure formation can be found in [10]. Other preferential freqencies with small peak pressures are refered to the vortex shedding frequencies from the main jet and reflection due to the reflecting boundaries. Unlike ρ' and p', there are no dominant frequencies identified

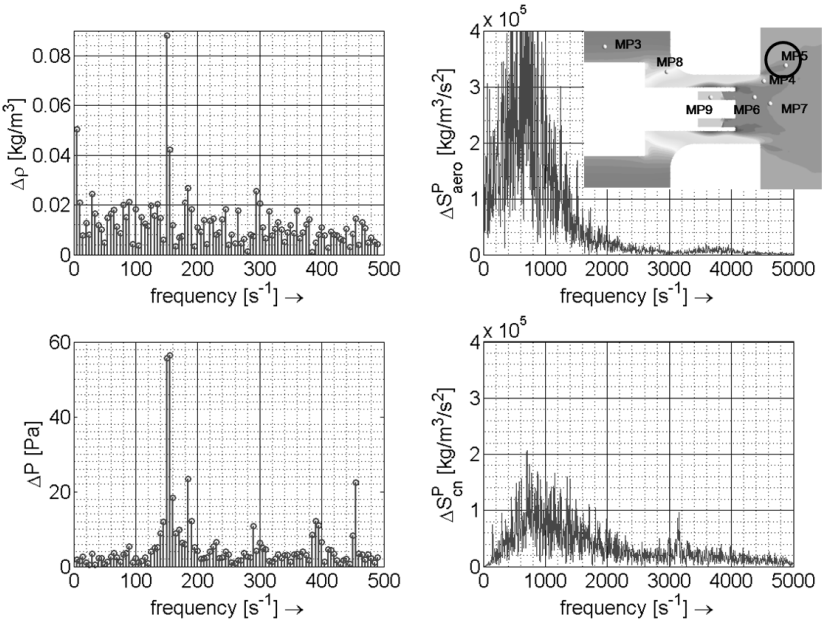

Fig. 2.30 Spectra of the monitor point in the main jet.

in the spectra of the two source terms. As strong turbulence is generated in the jet, the formulations of $S_{aero} = \frac{\partial^2}{\partial x_i \partial x_j}(\rho v_i v_j)$ and $S_{cn} = \frac{\partial^2}{\partial t^2}(p'/c_0^2 - \rho')$ implicitly represent the turbulence energy cascade, where vortices with a wide range in time and space exist. Therefore, the noise sources make a broadband spectrum from low to very high frequencies. Like a turbulent energy spectrum, the sources increases at first from $0Hz$, reach the peak values by about $700Hz - 900Hz$, and decrease again at high frequencies. Vortices with more than $f = 2500Hz$ turnover frequency do almost not contribute to S_{aero}. In contrast, there is a magnitude of S_{cn} in the high frequency region. This is because, although the small turbulent eddies (with high frequencies) carry only very little turbulent energy, the length scales of these eddies are still larger than the flame thickness, so that the flame front can be interacted by these small eddies and causes S_{cn}.

2.4 Conclusions

The investigations shown in the presented article cover detailed noise measurements of isothermal swirl flows and swirl flames (fully-premixed and non-premixed). The spectral analysis of pressure fluctuations shows explicit preferential frequencies for the isothermal and the reacting case (premixed conditions). As the source, coherent structures were detected. The underlying physical mechanism [10, 25] is the same for the isothermal and reacting flow.
The results of detailed noise measurements enable to correlate the total sound pressure level of swirl flames with its sources namely, turbulent flow (75 dB), combustion noise (+25 dB) and coherent flow structures (+2.5 dB), the latter being caused by an unfavorable burner exit geometry, that is, unfortunately, very common in industrial burner designs. The formation and reaction of these flow structures lead to an increase of SPL up to 5 dB for isothermal flow and up to 3 dB for swirl flames. Their prevention results in a significant decrease of combustion noise.
The part of the total sound emission caused by the turbulent flow (isothermal or with reaction) is given by the turbulent swirl flow with its benefits e.g. the fast, turbulent mixing or the flame ignition stability, and cannot be reduced significantly by design modifications. The additional noise, generated by reacting coherent structures (here: oscillation of the axial position of the inner recirculation zone), indeed, is avoidable without any loss of the above mentioned benefits of turbulent swirl flames.
The investigation of non-premixed flames showed the necessity of a stable and stationary ignition zone to prevent additional noise through fluctuations of the ignition point leading to an increase of the combustion noise of 3 dB. Numerical simulations (LES) have also been performed to study the flow field of this burner with and without reaction. The TFC (turbulent flame speed closure) model has been proposed in combination with the Schmid model to compute premixed flame. The comparisons of the LES results with the measured mean flow variables showed good agreement. Coherent structures have been identified in the experiment using the burner exit geometry with a recessed pilot lance and it has been numerically proved. The Lighthill's acoustic analogy was taken into account to evaluate the noise sources generated by the swirl burner. The contributions of the different components of the Lighthill tensor have been illustrated and compared by visualization of the LES result. The noise sources generated by the combustion process are significantly larger than the sources caused by the turbulence. The results of these LES-simulations will be used as input data to calculate the combustion noise using the CAA method (Computational Aero-Acoustics). A spectral analysis for several monitor points within the flow domain has been made to analyse the flow/combustion dynamics. Dominant frequencies in the spectra of the density and the pressure fluctuations were identified to be the eigenfrequency of the burner and the frequency of the oscillating inner recirculation zone (IRZ).

Acknowledgements The authors gratefully acknowledge the financial support by the German Research Council (DFG) through the Research Unit FOR 486 "Combustion Noise".

References

[1] Bai T, Cheng, XC, Daniel BR, Jagoda JI, Zinn BT (1993) Vortex shredding and periodic combustion processes in a Rijke type pulse combustor, Combustion Science Technology, 94, 245-258
[2] Bamberger A (2004) Vortex sound of flutes observed with Particle Image Velocimetry. ICA conference, Kyoto
[3] Bender C, Büchner H (2005) Mechanismen der Lärmentstehung in freibrennenden und eingeschlossenen Drallflammen, VDI-Berichte: 22. Deutscher Flammentag-Verbrennung und Feuerungen, 1888, 311-317
[4] Bender C, Büchner H (2005) Noise emissions from a premixed swirl combustor, Proceedings of Twelfth International Congress on Sound and Vibration (ICSV 12), CD-ROM.
[5] Beer JM, Chigier NA (1972) Combustion aerodynamics, Applied Science Publisher, London
[6] Brick H, Piscoya R, Ochmann M, Költzsch P (2005) Prediction of the Sound Radiated from Open Flames by Coupling a Large Eddy Simulation and a Kirchhoff-Method. Proc. Forum Acusticum, 85-89, Budapest
[7] Bui TP, Schröder W, Meinke M (2007) Acoustic perturbation equations for reacting flows to compute combustion noise. International Journal of Aeroacoustics, volume 6, nr.4
[8] Bui TP, Meinke M, Schröder W (2004) A Hybrid Approach to Analyze the Acoustic Field Based on Aerothermodynamic Effects. Proc. Joint Congress CFA/DAGA'04, Strasbourg, France, 121-122
[9] Büchner H (1992) Entstehung und theoretische Untersuchungen der Entstehungsmechanismen selbst-erregter Druckschwingungen in technischen Vormisch-Verbrennungssystemen, PhD Thesis, University of Karlsruhe
[10] Büchner H, Lohrmann M (2003) Coherent Flow Structures in Turbulent Swirl Flames as Drivers for Combustion Instabilities. Proc. Intern. Colloquium on Combustion and Noise Control
[11] Cabana M, Fortune V, Jordan P (2006) A look insight the Lighthill source term. 12th AIAA/CEAS Aeroacoustics Conference. Cambridge, MA, USA, AIAA-2006-2484
[12] Catlin J B, Day W H, Goom K (1999) The Pratt & Whitney Industrial Gas Turbine Product Line, Proc. of Power Gen Conference
[13] Colin O, Ducros F, Veynante D, Poinsot T (2000) A thickened flame model for large eddy simulations of turbulent premixed combustion. Phys. Fluids. 12, 7
[14] Duchamp de Lageneste L, Pitsch H (2001) Progress in large-eddy simulation of premixed and partially-premixed turbulent combustion. Center for Turbulence Research, Annual Research Briefs
[15] Fröhlich J (2006) Large Eddy Simulation turbulenter Strömungen, ISBN-10 3-8351-0104-8
[16] Gupta AK, Lilley DG, Syred N (1984) Swirl Flows, Abacus Press, Kent(U.K.)

[17] Habisreuther P, Bender C, Petsch O, Büchner H, Bockhorn H (2004) Calculated and Measured Turbulent Noise in a Strongly Swirling Isothermal Jet, Proceedings Joint Congress CFA/DAGA, 1179-1180
[18] Habisreuther P, Bender C, Petsch O, Buechner H, Bockhorn H (2006) Prediction of Pressure Oscillations in a Premixed Swirl Combustor Flow and Comparison to Measurements. Flow Turbulence and Combustion
[19] Habisreuther P, Lischer T, Cai W, Krebs W, Zarzalis N (2007) Visualisation of statistically periodic coherent structures in turbulent flow using a phase locked averaging method. Progress in computational fluid dynamics
[20] Hermesmeyer, Prade, Gruschka, Schmitz, Hoffmann and Krebs(2002) V64.3A Gas Burner Natural Gas Burner Development, Proceedings of ASME Turbo Expo
[21] Keck O, Meier W, Stricker W, Aigner M (2002) Establishment of a confined swirling natural gas/air flame as standard flame: Temperature and species distribution from laser Raman measure-ments, Combustion Science Technology, 174(8), 117-151
[22] Kühlsheimer C, Büchner H (2002) Combustion Dynamics of Turbulent Swirling Flows, Combus-tion and Flame, 131 (1-2), 70-84
[23] Leuckel W, Fricker N(1976) The characteristics of swirl-stabilized natural gas flames. Part I: Dif-ferent flame types and their relation to flow and mixing patterns, J. Inst. Fuel, 49, 103-112
[24] Lighthill M J (1952) On sound generated aerodynamically I. General Theory. Proc. R. Soc. A211, 564-587
[25] Lohrmann M, Büchner H (2000) Periodische Störungen im turbulenten Strömungsfeld eines Vor-misch-Drallbrenners, Chem.-Ing. Technik 72, 512-515
[26] Pitsch H, Duchamp de Lageneste L (2002) Large-eddy simulation of premixed turbulent combustion using a level-set approach. Proceedings of the Combustion Institute, Volume 29
[27] Roux S, Lartique G, Poinsot T, Meier U, Berat C (2005) Studies of Mean and Unsteady Flow in a Swirled Combustor using Experiments, Acoustic Analysis and Large Eddy Simulations. Combustion and Flame (141) S.40-54
[28] Schadow K, Gutmark E, Parr T, Parr K, Wilson K, Crump J (1989) Large-scale coherent structures as drivers of combustion instability, Combustion Science Technology, 64, 167-186
[29] Schmid H P, Habisreuther P, Leuckel W (1998) A Model for Calculating Heat Release in Premixed Turbulent Flames, Combustion and Flame 113, pp. 79-91
[30] Selle L, Lartigue G, Poinsot T, Kaufmann P, Krebs W, Veynante D (2002) Large-eddy simulation of turbulent combustion for gas turbines with reduced chemistry. Center for Turbulence Research, Proceedings of the Summer Program
[31] Smagorinsky J (1963) General circulation experiments with the primitive equations I: The basic experiment. Mon. Weather Rev. 91, 99-164

[32] Wang P, Bai XS (2005) Large eddy simulation of turbulent premixed flames using level-set G-equation. Proceedings of the Combustion Institute 30, 583-591

[33] Zhang F, Habisreuther P, Hettel M, Bockhorn H (2008) Modeling of a Premixed Swirl-stabilized Flame Using a Turbulent Flame Speed Closure Model in LES. Flow, Turbulence and Combustion, Accepted.

[34] Ziegler G(1991) Entflammung magerer Methan/Luft-Gemische durch kurzzeitige Bogen- und Glimmentladung. PhD Thesis, University of Stuttgart

http://www.springer.com/978-3-642-02037-7

Combustion Noise
Schwarz, A.; Janicka, J. (Eds.)
2009, XVII, 291 p., Hardcover
ISBN: 978-3-642-02037-7